Strong Photonic Crystal Behavior in Regular Arrays of Core-Shell and Quantum Disc InGaN/GaN Nanorod LEDs

C. J. Lewins,[1, a)] E. D. Le Boulbar,[1] S. M. Lis,[1] P. R. Edwards,[2] R. W. Martin,[2] P. A. Shields,[1] and D. W. E. Allsopp[1, b)]

[1)] *Department of Electronic and Electrical Engineering, University of Bath, Claverton Down, Bath BA2 7AY, UK*

[2)] *Department of Physics, SUPA, University of Strathclyde, Glasgow, G4 0NG, UK*

(Dated: 24th July 2014)

We show that arrays of emissive nanorod structures can exhibit strong photonic crystal behavior, via observations of the far-field luminescence from core-shell and quantum disc InGaN/GaN nanorods. The conditions needed for the formation of directional Bloch modes characteristic of strong photonic behavior are found to depend critically upon the vertical shape of the nanorod sidewalls. Index guiding by a region of lower volume-averaged refractive index near the base of the nanorods creates a quasi-suspended photonic crystal slab at the top of the nanorods which supports Bloch modes. Only diffractive behavior could be observed without this region. Slab waveguide modelling of the vertical structure shows that the behavioral regime of the emissive nanorod arrays depends strongly upon the optical coupling between the nanorod region and the planar layers below. The controlled crossover between the two regimes of photonic crystal operation enables the design of photonic nanorod structures formed on planar substrates that exploit either behavior depending on device requirements.

PACS numbers: 78.67.Pt; 78.67.Uh

I. INTRODUCTION

Exploitation of photonic crystal (PhC) effects in light-emitting diodes (LEDs) has resulted in significant increases in light extraction efficiency[1–8], outperforming more commercialized surface roughening techniques[7]. In addition, PhC LEDs offer control over the direction in which the enhanced light extraction occurs[3,5,9,10]. The directivity of the light source is a significant limiting factor to performance in applications where the étendue of external optics is restrictive, notably display illumination and miniature projectors[11,12].

PhC LED designs typically operate in a diffractive or Bragg regime, where the regular nanostructure acts only as a perturbation to a slab waveguide, comprised of unpatterned epitaxial layers and often the substrate[6]. Light trapped in the laterally guided modes of this slab undergoes Bragg diffraction to the extraction cone by the PhC. Here, the periodic component of the wave function in each mode has only low overlap with the periodic medium and only weakly perturbs the waveguiding properties of the structure. This diffractive behavior has been observed and characterized in air-hole PhC LEDs with the PhC on the surface of the LED[2,5] and underneath the emitting region[13–15].

Another regime of operation exists, where the periodic component of the wave function instead dominates the behavior. In this case, the effect of diffraction or zone folding is sufficient to couple the optical states to their corresponding state inside the irreducible Brillioun zone, lifting the degeneracy between Brillioun zones. As a result, the allowed optical states in the nanostructured device are Bloch-like and the periodicity of the PhC strongly affects the light dispersion[6,8,16]. This 'strong' or Bloch regime of PhC operation is exploited to localize light in waveguiding applications[17,18]. However, its consideration for practical applications as a means of increasing the performance of LEDs[1,19–22] is limited to simulations or photoluminescence (PL) of suspended membrane air-hole PhC structures that are unsuitable for the electrical injection and heat extraction required.

Enhancement to the directivity of the emission using PhCs operating in the Bragg regime has been achieved through optimising the geometry of the LED and PhC[3,5,9,10]. However, the directionality that can be achieved using this method is fundamentally limited as light from slab modes will be diffracted to all angles from normal incidence[6]. These limitations can be overcome through operation in the Bloch regime to realize an ultra-directional light source[21].

More recently, PhC LED arrays of dielectric nanorods which contain the emitting region fabricated either by etching from pre-existing epitaxial layers or by bottom-up growth have become of interest. Two configurations for the emitting region have been reported: core-shell nanorod LEDs with the emitting region surrounding a nanorod core[23–26] and quantum disc nanorod LEDs with the rods intersecting a planar emission region[26–28]. The potential advantages of core-shell LEDs include providing a low cost means of fabricating non-polar LEDs in which the quantum-

[a)] C.J.Lewins@bath.ac.uk
[b)] D.Allsopp@bath.ac.uk

confined Stark effect. The increased area of the active region over its planar equivalent reduces the current density in the device and hence efficiency droop. Furthermore, the regrowth of active layer shells onto plasma-etched cores offers an effective route for highly-regular core-shell structures that show PhC effects[29]. Diffractive behavior has been observed in regular arrays of both quantum disc[28,30] and core-shell nanorod designs[29], both of which have been electrically-contacted successfully[24,28].

The Bloch PhC regime has been predicted theoretically to occur in a nanorod array LED with an underlying buffer layer and substrate[31]. However to date, despite the above advantages of nanorod array LEDs, this operating regime has proved hard to achieve in practice. As a result, nanorod LEDs formed on a planar substructure seem an ideal medium for exploring the scope for combining the practical advantages of nanorod arrays with the benefits offered by the Bloch regime of PhC operation.

This paper describes the experimental demonstration of the crossover from the Bragg to the Bloch regime of PhC operation in both core-shell and quantum disc nanorod array LED structures. The work also establishes an understanding of the physical conditions needed for manifesting the Bloch regime in practical nanorod LED structures.

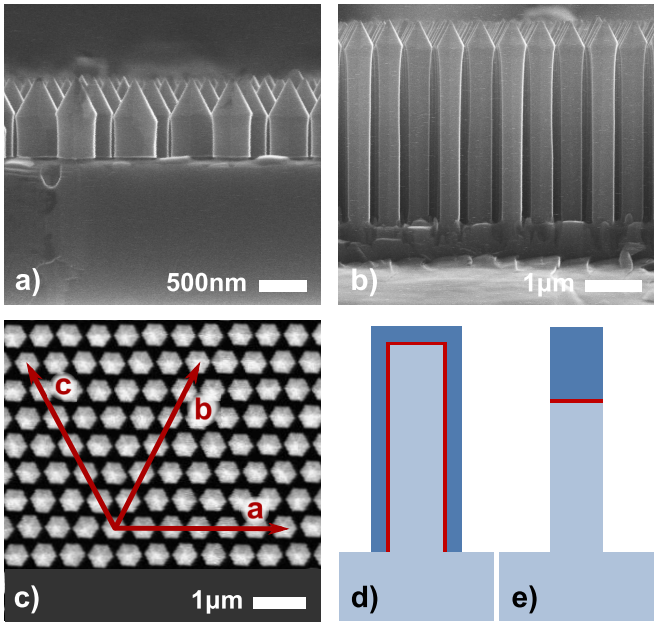

FIG. 1. Cross section of a) 850 nm and b) 4000 nm core-shell nanorods c) plan view of 4000 nm core-shell nanorods where the arrows indicate the lattice vectors. Schematic representation of d) core shell and e) quantum disc nanorod device configurations where red indicates the emitting region.

II. EXPERIMENTAL

A. Fabrication of core-shell and quantum disc nanorods

Two c-plane GaN-on-sapphire wafers with epitaxial GaN thicknesses of 2.1 and 5.5 μm were patterned with nickel nano-dots in a 600 nm pitch hexagonal lattice using nano-imprint lithography (NIL)[32]. These were inductively-coupled plasma (ICP) etched (Oxford Instruments ICP100) for different times to form GaN nanorods of height 500 and 3500 nm on the 2.1 and 5.5 μm templates respectively. GaN was regrown on the sidewalls and tips of the nanorods by metalorganic vapor phase epitaxy (MOVPE), creating nanorods with m-plane faceted sidewalls and $\{10\bar{1}1\}$ faceted pyramids on top[29]. A layer of InGaN was then grown, capped by another thin GaN layer, finally producing nanorods with heights of either 850 or 4000 nm with an underlying GaN buffer layer below of thickness 1650 and 2250 nm respectively. Figure 1 shows SEM images of the two core-shell samples after fabrication.

Quantum disc nanorod samples were defined by the same NIL process and dry-etched from an epitaxial structure comprising an n-type GaN layer, a 2nm thick single InGaN/GaN quantum well (SQW) with In fraction 15-20% and a 600 nm thick p-GaN layer grown on a 50 mm diameter sapphire wafer. The processing resulted in nanorods containing a disc-shaped SQW. This simpler structure was chosen for the investigation of photonic crystal effects in nanorod structures because the side-wall angle and nanorod height can be varied by controlling the ICP etching step[33].

B. Luminescent properties of nanorod LEDs

A 405nm diode laser was used to resonantly excite just the InGaN QW layers without significant absorption in the GaN layers. The core-shell nanorods were found to emit broadband photoluminescence (PL) at visible wavelengths, shown in figure 2a. There is a broad blue-green peak observed at 2.2-2.8 eV for both the 4000 nm and 850 nm core-shell nanorods which merges into another broad yellow emission band at 1.8-2.2 eV for the tall core-shell nanorods. The PL from the quantum disc nanorods also shown in figure 2a showed the single quantum well emission centred at 2.75 eV, along with broad yellow band emission below 2.6 eV.

To investigate the regions of the nanorods emitting luminescence, cathodoluminescence (CL) hyperspectral imaging with ≈20 nm spatial resolution was performed[34]. A 5 keV electron beam was scanned over the samples and the luminescence spectrum from each area of localized excitation measured. The CL results show that the blue-green emission observed in the PL of the core-shell nanorods is emitted from the base of the pyramids ≈500 nm from the tips of the rods and that the yellow emission is emitted from all areas. This is illustrated for the tall core-shell nanorods in figure 2b, which shows a real color representation of the excited luminescence, formed by calculating the chromacity coordinates from the mea-

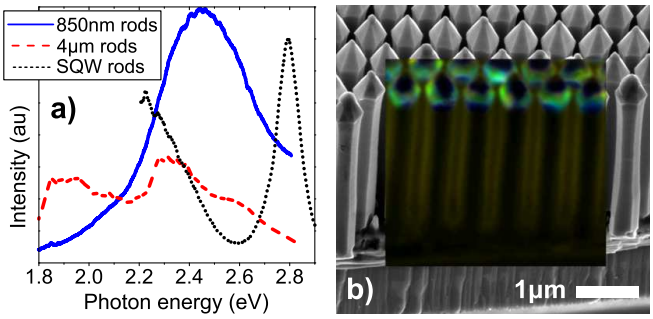

FIG. 2. a) PL spectra of core-shell (850 & 4000 nm high) and quantum disc (SQW) nanorods at normal incidence. b) (Color online) Real color representation of spatially resolved CL emission from 4000 nm core-shell nanorods.

sured spectrum at each position. The CL showed that the InGaN growth rate was higher around the base of the pyramids with a rapidly decreasing InN mole fraction down the nanorod sidewalls for the MOVPE growth conditions used. Comparable behavior was observed in the short core-shell nanorods[29]. Hyperspectral CL measurements on the quantum disc nanorods showed that the emission comprised a peak at ≈2.8 eV associated with the SQW and located at 600 nm below the nanorod tips with yellow band emission from all areas.

C. Angular luminescence of core-shell nanorod LEDs

The angular distribution of the far-field intensity of the PL from the various nanorod structures was measured. The measurement system comprised a spectrometer coupled to a 0.22 NA optical fibre bundle which was moved over the hemisphere above the device at a radius of 300 mm and with angular resolution of 0.1° in both the azimuthal and inclinal directions[15]. Most data were obtained at 0.2° resolution, but were supplemented by higher resolution measurements performed at fixed azimuth, with the inclinal angle varied from surface normal to 90° at an angular resolution of 0.1°.

Figure 3a shows the k-space projection of the variation in the luminescence with inclinal observation angle for the 850 nm core-shell nanorods. The measurement was performed along the azimuthal direction of lattice vector **a** shown in figure 1c and defined as the $\mathbf{\Gamma K_a}$ direction in reciprocal space. The k-space projection was performed by converting photon energy into freespace wavenumber (k_0), which is plotted on the vertical axis, and by plotting along the horizontal axis the in-plane component of k_0 given by $k_{||} = k_0 \sin\theta$ where θ is the angle between the propagation direction and the surface normal. The intensity variation has been normalized to enhance the contrast of the features by correcting for the gross variation in intensity with angle from surface normal and then dividing each spectrum by the mean intensity at each wavelength.

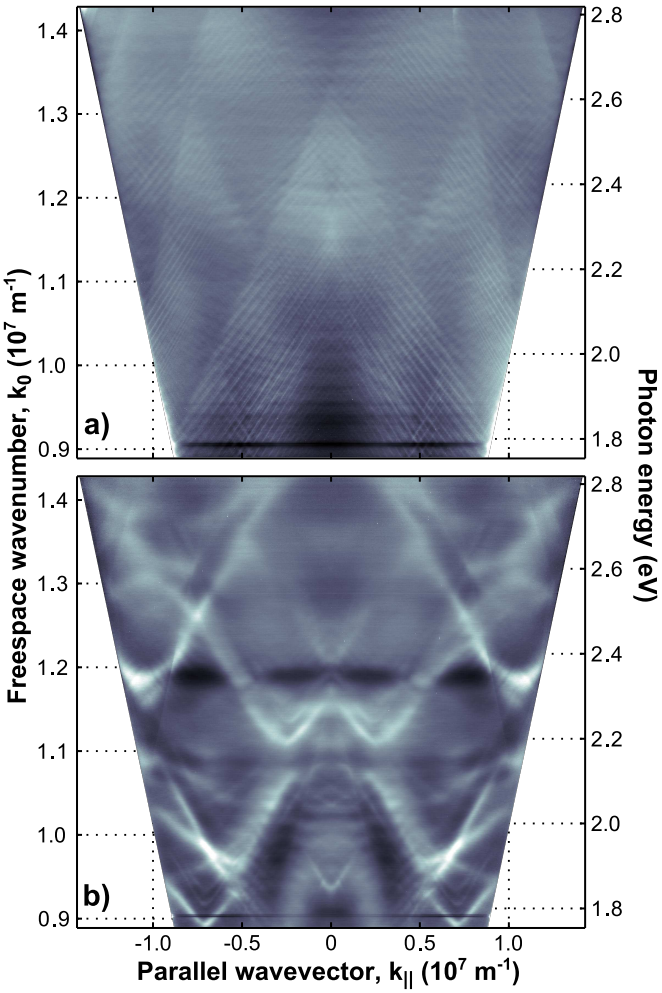

FIG. 3. Normalized k-space projection showing the angular PL intensity variation with frequency and inclinal angle along the $\mathbf{\Gamma K_a}$ direction for the a) 850 nm and b) 4000 nm tall core-shell nanorods

The k-space projection is characterized by sets of sharp white lines that correspond to diffraction by the nanorod array. These lines arise from light coupled into the slab modes of the GaN buffer layer being diffracted into the extraction cone. Each line originates from diffraction out of a particular slab mode and is replicated at different observation angles corresponding to the different diffraction orders. The effective refractive indices of these modes were found to lie between that of the sapphire substrate (≈1.8) and the GaN buffer layer (≈2.4) at 2.16 eV, confirming they originate from this family of slab modes[15].

A further diffractive effect is apparent from guided modes with effective indices of less than ≈1.8, indicating that these propagate in the sapphire substrate. The spacing of these modes is too close to resolve owing to the large thickness of the sapphire substrate. Rather, they give rise to the triangular sectors which correspond to band folding (i.e. diffraction) of the air and sapphire extraction cones, for example at $|k_{||}| < 0.25 \times 10^7$ m^{-1}

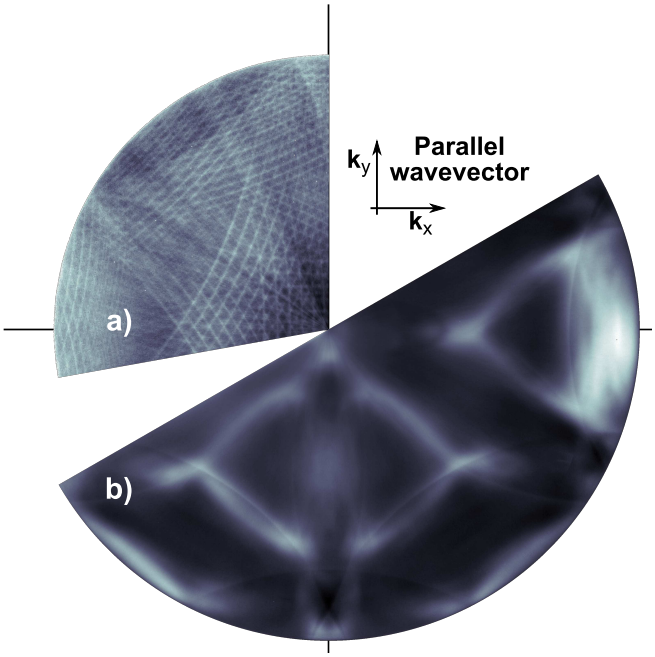

FIG. 4. Normalized in-plane k-space projection of angular PL showing the intensity variation with azimuth and inclinal angle for a single frequency at a) $k_0 = 1.05 \times 10^7$ m^{-1} (2.07 eV) from the 850 nm tall core-shell nanorods and b) $k_0 = 1.19 \times 10^7$ m^{-1} (2.34 eV) from the 4000 nm tall core-shell nanorods. k_x is parallel to the $\mathbf{\Gamma K_a}$ direction.

at ≈2.4 eV in figure 3a. Competition between diffraction orders causes the sharp variations in the intensity of the substrate and discrete guided modes at the boundaries of the triangular sectors. This is because another route becomes available for diffraction as each mode passes into the extraction cones, so the power is distributed between the various extraction routes.

Figure 4a shows an in-plane k-space projection in (k_x, k_y), constructed from measurements taken over 100° of azimuth and 90° of angle from surface normal at a single photon energy of $k_0 = 1.05 \times 10^7$ m^{-1} (2.07 eV). The sharp white lines created by the light diffracted from the discrete guided modes are observed as arcs centred on the reciprocal lattice points of the photonic crystal. Before diffraction, these modes (arcs) have a magnitude of in-plane wave vector (radius) which does not vary with azimuthal direction. This confirms that the 850 nm core-shell nanorods are operating in the diffractive Bragg regime, where the nanorod PhC structure acts as a perturbation of a homogeneous slab waveguide[6,8,15].

Figure 3b shows the k-space projection of the angular PL from the 4000 nm core-shell nanorods along the $\mathbf{\Gamma K_a}$ direction. The dense array of features deriving from the diffraction in the far field emission from the 850 nm core-shell nanorods no longer occurs and a very different behavior is observed. Light emission is observed in broad, widely separated bands of varying intensity with both crossings and anti-crossings of these bands occurring: behavior characteristic of the Bloch regime[6,8]. Further, these broad features were observed to vary with azimuthal direction in a pattern consistent with the reciprocal lattice of the PhC, as shown in the in-plane k-space intensity plot for $k_0 = 1.19 \times 10^7$ m^{-1} (2.34 eV) presented as figure 4b. This correlation of the band structure with the symmetry of the PhC tiling demonstrates that these bands derive from Bloch modes folded into the air cone. Precise characterisation of these modes is challenging due to a distortion from a regular hexagonal tiling introduced during fabrication and the several orders of band folding possible at the 600 nm pitch for the emitted photon energies measured[35].

These observations show, possibly for the first time, that the Bloch regime can occur in practical nanorod LED structures comprising of finite nanorods supported by a higher average refractive index buffer layer. The more conventional Bragg regime was also observed. There are two significant differences between the two core-shell nanorod samples, either of which could be responsible for the observed change in PhC behavior. Firstly, the samples are different heights and secondly, they have a different vertical profile as seen in the SEM images in figure 1.

D. Dependence of photonic crystal behavior on nanorod geometry

The origin of this change in behavior in nanorod LEDs was explored further by performing the same measurements on arrays of quantum disc nanorods with different heights and vertical profiles.

A matrix of four quantum disc nanorod samples was created by using two different etch depths with either undercut (negative sidewall angle) or tapered (positive sidewall angle) vertical profiles. The measured parameters of these nanorods are shown in table I and cross section SEM images in figure 5.

Figure 5 also shows k-space projections of the angular PL observed along the $\mathbf{\Gamma K_a}$ direction for each sample. Samples SQW1 and SQW3 with a tapered vertical profile show diffractive behavior, which occurs irrespective of nanorod height. However, samples SQW2 and SQW4 with an undercut profile show broad white lines indicative of Bloch mode formation superimposed over much weaker diffractive behavior. From these results, it is concluded that the vertical geometry determines whether nanorod array LEDs behave in the Bragg or Bloch PhC regime. On the other hand, the change of height has a lesser effect on the characteristics of the behavior since diffraction is prominent in both the 1700 nm (SQW1) and 3050 nm (SQW3) tall nanorod samples.

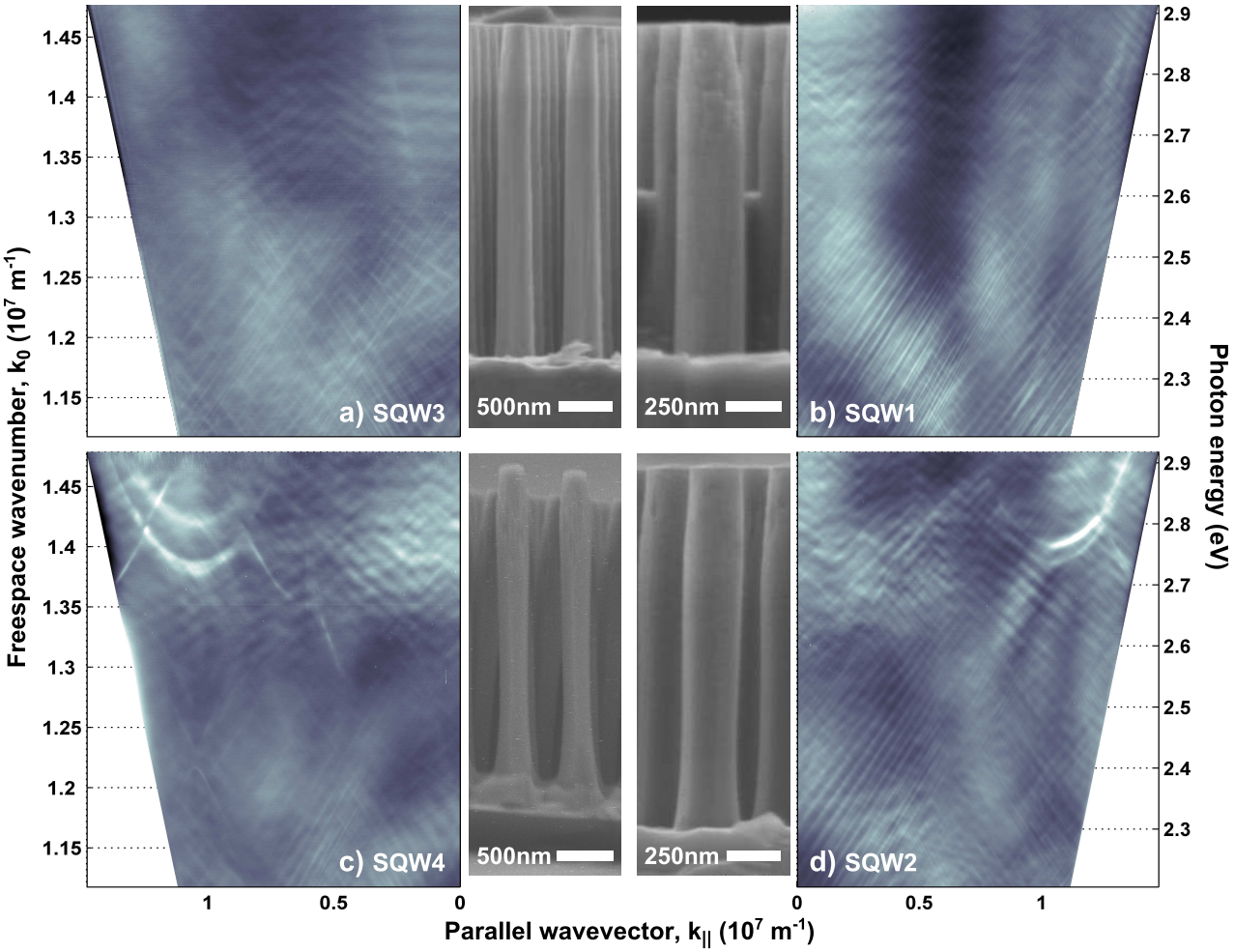

FIG. 5. Cross section SEM images and k-space projection of the angular PL intensity variation along the $\mathbf{\Gamma K_a}$ direction for a) SQW3, tapered 3050 nm, b) SQW1 tapered 1700 nm, c) SQW4 undercut 3175 nm, d) SQW2 undercut 1800 nm high rods.

TABLE I. Characteristics of quantum disc nanorod samples

Sample	GaN buffer depth (nm)	Nanorod height (nm)	Vertical profile
SQW1	3900	1700	Tapered
SQW2	3800	1800	Undercut
SQW3	2600	3050	Tapered
SQW4	2600	3175	Undercut

III. ANALYSIS AND DISCUSSION

The vertical profile of the nanorods leads to a variation in the air filling fraction of the array with vertical position in the nanorod. If the nanorods are considered as an effective bulk medium for in-plane directions, the vertical variation in effective refractive index can be estimated by volume-averaging the dielectric constant in steps up the nanorods[36]. Previous work has shown this is a valid approximation for a periodic medium for the length scales and wavelengths considered in these samples[15,31]. Curves (i-iii) in figure 6c show the refractive index variation with vertical position for the samples with an undercut profile, calculated by extracting the fill factor variation with vertical position from the SEM images. There is a region of higher volume-averaged refractive index bounded above and below by regions of lower volume-averaged refractive index. Such a structure is reminiscent of a suspended slab waveguide which is optically decoupled from the GaN buffer layer, or partially so. In essence, a quasi-suspended photonic crystal slab waveguide is formed. For some in-plane wave-vectors this provides an index-guiding mechanism that confines light to the periodic medium, thus enabling Bloch modes to form along particular directions.

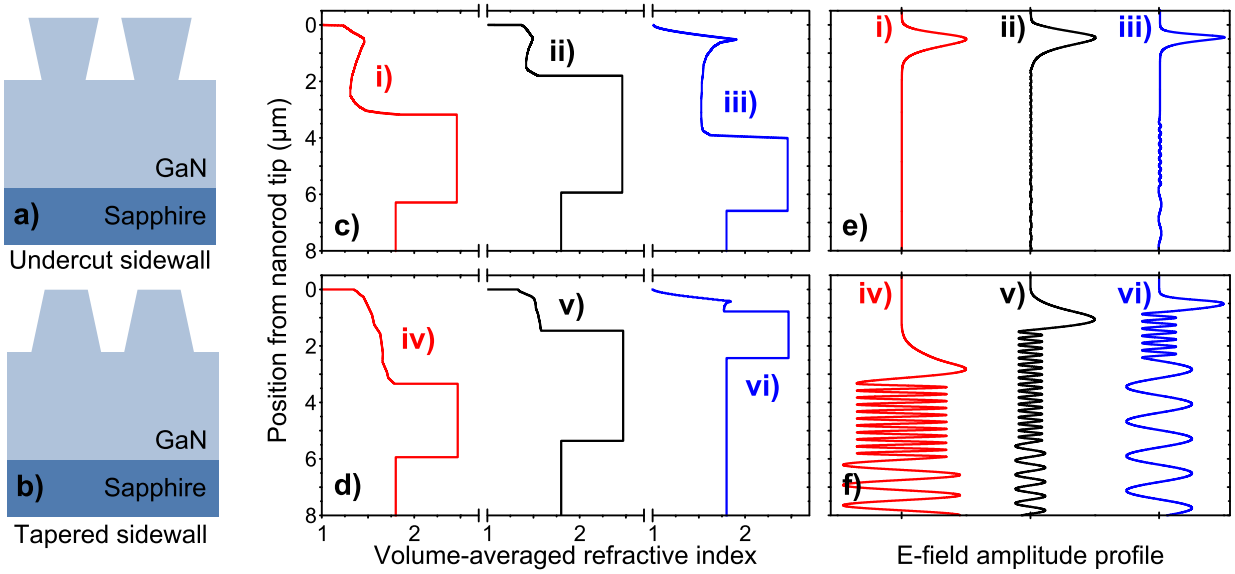

FIG. 6. Schematic representation of nanorod arrays with (a) undercut and (b) tapered sidewalls. Volume-averaged refractive index profiles (c,d) and modelled **E**-field amplitude profile (e,f) of the first-order resonance in the PhC region for i) 3175 nm tall rods with undercut sidewalls (SQW4), ii) 1800 nm tall rods with undercut sidewalls (SQW2), iii) 4000 nm tall core-shell rods, iv) 3050 nm tall rods with tapered sidewalls (SQW3), v) 1700 nm tall rods with tapered sidewalls (SQW1) and vi) 850 nm tall core-shell rods.

The variation of the volume-averaged dielectric constant with vertical position was used to construct a slab-waveguide model for the structures, which was solved using a transfer matrix method[37]. This model is able to show the degree of optical coupling between the quasi-suspended PhC slab and the GaN buffer layer, although it cannot provide information about the azimuthal variation in the parallel wave-vectors for the Bloch modes. A staircase approximation for the volume-averaged refractive index in the vertical direction was used with a 20 nm ($\ll \lambda$) resolution.

Examining the optical mode profiles of the resonances in the system allows the index guiding to be investigated. These are shown in figure 6e and 6f. For the samples with the undercut profile (fig. 6e), modes with their optical energy confined in the photonic crystal layer by total internal reflection are supported, as expected from the volume-averaged refractive index variation with vertical position. The electric field variation for the first order TE modes in the PhC layer in the undercut nanorods is shown in curves (i-iii) in figure 6e where it can be seen that the field is negligible in the GaN buffer layer. Optical energy in these modes is only subject to loss from the periodic region due to photon recycling or scattering from non-ideal surfaces and band folding to wave-vectors outside the guided range in the extraction cone.

In contrast, curves (iv-v) in figure 6f show the field profiles of the first order resonances in the quantum disc nanorods with the tapered profiles. All the light emitted into states that propagate in the PhC region can now be readily coupled into the substrate and is only confined in the PhC by non-total Fresnel reflection at the interface with the GaN buffer. The absence of Bloch-like bands in the angular PL results from the tapered samples (figs 5a-b) indicates that this confinement mechanism is too lossy in these samples to support the formation of Bloch modes.

In the case of the 4000 nm core-shell rods (see fig. 3b), the Bloch features are very strong and appear in several bands that extend over large ranges of emission angle, and no Bragg diffraction is observed in this sample. In contrast, the band structure for both the undercut SQW samples (see fig. 5c-d) is less striking. For the taller core-shell geometry, the slab waveguide model predicts the existence of three TE modes with their field amplitude almost entirely confined to the PhC layer, whereas only one confined TE mode for both the undercut SQW samples is predicted. Consequently, light is guided in the quasi-suspended PhC slab formed in the 4000 nm core-shell nanorods for a much wider range of in-plane wave-vector ($k_{||}$) or effective refractive index than in the two undercut SQW nanorod samples, as expected from the variation of the volume-averaged refractive index with vertical position (see fig. 6c). The wider range of guided wave-vectors gives rise to a higher photonic density of states associated with the Bloch modes, which results in the richer spectrum of photonic bands observed. In contrast, the smaller range of wave-vectors for which modes are guided in the slab in the undercut SQW nanorods results in the fewer bands observed.

The difference in the broadness of the resonance lines seen in the core-shell and quantum disc nanorods represents a difference in optical loss from the modes, with a broader line representing a larger loss. The Bloch modes

in the core-shell nanorods could be broader due to higher diffraction efficiency for this structure or it could be due to the light absorbing volume being larger than in the quantum disc nanorods, leading to increased loss through photon recycling.

The variation in the strength of the diffractive features in the undercut samples can be understood by considering that there is a ≈2000 nm wide region of lower volume-averaged refractive index between the quasi-suspended PhC slab formed in the taller core-shell nanorods and the underlying GaN buffer. This optical barrier region effectively decouples the two waveguiding regions, leading to little interaction between the layers and prevents any substantial leakage of optical power into GaN buffer slab modes. As a result, features created by diffraction are not observed in the tall core-shell structures. The slight undercut and the small separation between the waveguides seen in the 850 nm core-shell nanorods is not sufficient to decouple the PhC region from the GaN buffer, as seen in the E-field magnitude profile shown in curve (vi) in figure 6f.

Further, the k-space plots from the SQW nanorod samples provide additional evidence to support this two-waveguide model. The Bloch modes in figure 5 are stronger for the blue QW emission band (2.6–2.9 eV) than for the yellow band emission (<2.6 eV). This occurs because the QW is located in the region of lower air fill and so its emission will couple readily into the quasi-suspended slab. In contrast, the yellow band is not localized to this region and so is more able to couple directly to the GaN buffer layer slab modes rather than the Bloch modes, causing the retention of strong Bragg diffractive features at lower photon energies. Thus locating the emissive region in a nanorod or core-shell LED in a quasi-layer of lower air fill will enhance the likelihood of Bloch mode formation.

IV. CONCLUSION

Ordered arrays of shaped nanorod LEDs on a planar substrate have been observed to operate in the Bloch regime through far-field angular photoluminescence measurements, revealing laterally-guided directional Bloch modes folded to the air extraction cone. This result shows that the behavior of the Bloch regime can be exploited in emissive devices without requiring a suspended membrane structure.

The condition required to manifest the Bloch regime is for optical losses from guided Bloch modes to be limited. This is achieved most readily by coupling light into modes that are confined to a periodic layer by index guiding in a vertical direction. In this work, the air fill fraction of nanorod LED arrays was varied with vertical position to produce regions of high fill fraction bounded by regions of lower fill, creating in effect a quasi-suspended photonic crystal slab in which Bloch modes readily undergo index guiding. Control of optical losses through coupling to the underlying buffer layer was achieved by varying the height and the fill fraction of the region of higher air fill in the nanorods.

Slab-waveguide modelling showed that the strength of the features in different experimental geometries correlates with the optical coupling between the quasi-suspended photonic crystal slab and the planar buffer layer; a larger distance and refractive index contrast between the two guiding regions leads to more pronounced Bloch regime behavior. Tapered nanorods with a positive sidewall angle display more conventional Bragg diffractive behavior, in line with previous results. Finally, the results show that both quantum disc and core-shell nanorod arrays can be designed and fabricated to enable the exploitation of either Bloch or diffractive behavior in photonic devices according to their application. By varying the shape of the nanorod sidewalls, the advantages of both the Bragg diffractive and Bloch photonic crystal operating regimes can be combined with the advantages of core-shell and quantum disc nanorod LEDs.

ACKNOWLEDGMENTS

The authors wish to acknowledge funding support from the U.K. Engineering and Physical Sciences Research Council (EPSRC) under Grant EP/1012591 'Lighting the Future', the EPSRC doctoral training awards and Osram Opto Semiconductors GmbH for the provision of the GaN/sapphire templates through the European Union FP7 'SMASH' programme (Contract No. 228999).

[1] S. Fan, P. Villeneuve, J. Joannopoulos, and E. Schubert, "High extraction efficiency of spontaneous emission from slabs of photonic crystals," Physical Review Letters **78**, 3294–3297 (1997).

[2] T. N. Oder, J. Shakya, J. Y. Lin, and H. X. Jiang, "III-Nitride Photonic Crystals," Applied Physics Letters **83**, 1231–1233 (2003).

[3] J. J. Wierer, M. R. Krames, J. E. Epler, N. F. Gardner, M. G. Craford, J. R. Wendt, J. A. Simmons, and M. M. Sigalas, "InGaN/GaN Quantum-Well Heterostructure Light-Emitting Diodes Employing Photonic Crystal Structures," Applied Physics Letters **84**, 3885–3887 (2004).

[4] M. Charlton, T. Lee, M. Zoorob, P. Shields, and W. Wang, "Improving LED extraction efficiency through surface patterning," in *Proceedings of SPIE*, Vol. 6669 (Spie, 2007) pp. 666914–666914–7.

[5] P. Shields, M. Charlton, T. Lee, M. Zoorob, D. Allsopp, and W. Wang, "Enhanced Light Extraction by Photonic Quasi-Crystals in GaN Blue LEDs," IEEE Journal of Selected Topics in Quantum Electronics **15**, 1269–1274 (2009).

[6] C. Wiesmann, K. Bergenek, N. Linder, and U. Schwarz, "Photonic crystal LEDs - designing light extraction," Laser & Photonics Review **3**, 262–286 (2009).

[7] J. J. Wierer, A. David, and M. M. Megens, "III-Nitride Photonic-Crystal Light-Emitting Diodes with High Extraction Efficiency," Nature Photonics **3**, 163–169 (2009).

[8] A. David, H. Benisty, and C. Weisbuch, "Photonic crystal light-emitting sources," Reports on Progress in Physics **75**, 126501 (2012).

[9] C. Lai, H. Kuo, C.-H. Chao, P. Yu, and W. Yeh, "Structural Effects on Highly Directional Far-Field Emission Patterns of GaN-Based Micro-Cavity Light-Emitting Diodes With Photonic Crystals," Journal of Lightwave Technology **28**, 2881–2889 (2010).

[10] E. Rangel, E. Matioli, Y.-S. Choi, C. Weisbuch, J. S. Speck, and E. L. Hu, "Directionality control through selective excitation of low-order guided modes in thin-film InGaN photonic crystal light-emitting diodes," Applied Physics Letters **98**, 081104 (2011).

[11] G. Harbers, S. J. Bierhuizen, and M. R. Krames, "Performance of High Power Light Emitting Diodes in Display Illumination Applications," Journal of Display Technology **3**, 98–109 (2007).

[12] A. Wilm, "Requirements on LEDs in etendue limited light engines," Proc. of SPIE, Photonics in Multimedia II **7001**, 70010F–70010F–10 (2008).

[13] M.-K. Kwon, J.-Y. Kim, I.-K. Park, K. S. Kim, G.-Y. Jung, S.-J. Park, J. W. Kim, and Y. C. Kim, "Enhanced emission efficiency of GaN/InGaN multiple quantum well light-emitting diode with an embedded photonic crystal," Applied Physics Letters **92**, 251110 (2008).

[14] E. Matioli and C. Weisbuch, "Impact of photonic crystals on LED light extraction efficiency: approaches and limits to vertical structure designs," Journal of Physics D: Applied Physics **43**, 354005 (2010).

[15] C. J. Lewins, D. W. E. Allsopp, P. A. Shields, X. Gao, B. Humphreys, and W. N. Wang, "Light Extracting Properties of Buried Photonic Quasi-Crystal Slabs in InGaN/GaN LEDs," Journal of Display Technology **9**, 333–338 (2013).

[16] E. Yablonovitch, "Inhibited spontaneous emission in solid-state physics and electronics," Physical Review Letters **58**, 2059–2062 (1987).

[17] S. Johnson, P. Villeneuve, S. Fan, and J. Joannopoulos, "Linear waveguides in photonic-crystal slabs," Physical Review B **62**, 8212–8222 (2000).

[18] C. Jamois, R. Wehrspohn, L. Andreani, C. Hermann, O. Hess, and U. Gösele, "Silicon-based two-dimensional photonic crystal waveguides," Photonics and Nanostructures - Fundamentals and Applications **1**, 1–13 (2003).

[19] M. Boroditsky, T. F. Krauss, R. Coccioli, R. Vrijen, R. Bhat, and E. Yablonovitch, "Light extraction from optically pumped light-emitting diode by thin-slab photonic crystals," Applied Physics Letters **75**, 1036 (1999).

[20] R. K. Lee, Y. Xu, and A. Yariv, "Modified spontaneous emission from a two-dimensional photonic bandgap crystal slab," Journal of the Optical Society of America B **17**, 1438–1442 (2000).

[21] A.-L. Fehrembach, S. Enoch, and A. Sentenac, "Highly Directive Light Sources Using Two-Dimensional Photonic Crystal Slabs," Applied Physics Letters **79**, 4280–4282 (2001).

[22] M. Fujita, S. Takahashi, Y. Tanaka, T. Asano, and S. Noda, "Simultaneous inhibition and redistribution of spontaneous light emission in photonic crystals," Science **308**, 1296–1298 (2005).

[23] F. Qian, S. Gradecak, Y. Li, C.-Y. Wen, and C. M. Lieber, "Core/multishell nanowire heterostructures as multicolor, high-efficiency light-emitting diodes." Nano Letters **5**, 2287–2291 (2005).

[24] A.-L. Bavencove, D. Salomon, M. Lafossas, B. Martin, A. Dussaigne, F. Levy, B. Andre, P. Ferret, C. Durand, J. Eymery, L. S. Dang, and P. Gilet, "Light emitting diodes based on GaN core/shell wires grown by MOVPE on n-type Si substrate," Electronics Letters **47**, 765–766 (2011).

[25] J.-R. Chang, S.-P. Chang, Y.-J. Li, Y.-J. Cheng, K.-P. Sou, J.-K. Huang, H.-C. Kuo, and C.-Y. Chang, "Fabrication and luminescent properties of core-shell InGaN/GaN multiple quantum wells on GaN nanopillars," Applied Physics Letters **100**, 261103 (2012).

[26] S. Li and A. Waag, "GaN based nanorods for solid state lighting," Journal of Applied Physics **111**, 071101 (2012).

[27] C. Kolper, W. Bergbauer, P. Drechsel, M. Sabathil, M. Strassburg, H.-J. Lugauer, B. Witzigmann, S. Fundling, S. Li, H.-H. Wehmann, and A. Waag, "Towards nanorod LEDs: Numerical predictions and controlled growth," Physica Status Solidi (C) **8**, 2305–2307 (2011).

[28] Y. Zhuang, C. Lewins, S. Lis, P. Shields, and D. Allsopp, "Fabrication and Characterization of Light Emitting Diodes Comprising Highly Ordered Arrays of Emissive InGaN/GaN Nanorods," IEEE Photonics Technology Letters **25**, 1047–1049 (2013).

[29] E. D. Le Boulbar, I. Gîrgel, C. J. Lewins, P. R. Edwards, R. W. Martin, A. Šatka, D. W. E. Allsopp, and P. A. Shields, "Facet recovery and light emission from GaN/InGaN/GaN core-shell structures grown by metal organic vapour phase epitaxy on etched GaN nanorod arrays," Journal of Applied Physics **114**, 094302 (2013).

[30] S. Keller, C. Schaake, N. A. Fichtenbaum, C. J. Neufeld, Y. Wu, K. McGroddy, A. David, S. P. DenBaars, C. Weisbuch, J. S. Speck, and U. K. Mishra, "Optical and structural properties of GaN nanopillar and nanostripe arrays with embedded InGaN/GaN multi-quantum wells," Journal of Applied Physics **100**, 054314 (2006).

[31] A. David, H. Benisty, and C. Weisbuch, "Spontaneous emission in GaN/InGaN photonic crystal nanopillars," Opt. Express **15**, 871–880 (2007).

[32] P. A. Shields and D. W. Allsopp, "Nanoimprint lithography resist profile inversion for lift-off applications," Microelectronic Engineering **88**, 3011–3014 (2011).

[33] P. Shields, M. Hugues, J. Zúñiga Pérez, M. Cooke, M. Dineen, W. Wang, F. Causa, and D. Allsopp, "Fabrication and properties of etched GaN nanorods," Physica Status Solidi (C) **9**, 631–634 (2012).

[34] P. R. Edwards and R. W. Martin, "Cathodoluminescence nanocharacterization of semiconductors," Semiconductor Science and Technology **26**, 064005 (2011).

[35] The roller NIL process used produced an asymmetric pattern distortion to the hexagonal tiling of the nanorods as shown in figure 1c. Relative to the lattice vectors **a**, **b** and **c** illustrated in figure 1c the distortion resulted in a 10% elongation in the **b** and **c** direction relative to **a**, which is at the intended 600 nm pitch.

[36] D. Aspnes, "Local-field effects and effective-medium theory: a microscopic perspective," American Journal of Physics **50**, 704–709 (1982).

[37] P. Yeh, *Optical Waves in layered media* (Wiley, Hoboken, NJ, 2005) p. 416.